Supported Gold Nanoparticles from Quantum Dot to Mesoscopic Size Scale: Effect of Electronic and Structural Properties on Catalytic Hydrogenation of Conjugated Functional Groups

Peter Claus,*,† Angelika Brückner,‡ Christian Mohr,‡ and Herbert Hofmeister§

Contribution from the Department of Chemistry, Institute of Chemical Technology II, Darmstadt University of Technology, Petersenstrasse 20, D-64287 Darmstadt, Germany, Department of Catalysis, Institute for Applied Chemistry, Richard-Willstätter-Strasse 12, D-12489 Berlin, Germany, and Max Planck Institute of Microstructure Physics, Weinberg 2, D-06120 Halle, Germany

Received April 13, 2000

Abstract: Titania- and zirconia-supported gold particles of 1−5 nm size, prepared by various routes of synthesis, were employed in the partial hydrogenation of acrolein. In-depth characterization of their structural and electronic properties by electron microscopy, electron paramagnetic resonance, and optical absorption spectroscopy aimed at disclosing the nature of the active sites controlling the hydrogenation of C=O vs C=C bonds. The structural characteristics of the catalysts, as mean particle size, size distribution, and dispersion, distinctly depend on the synthesis applied and the oxide support used whereby the highest gold dispersion ($D_{Au} = 0.78$, Au/TiO_2) results from a modified sol−gel technique. For extremely small gold particles on titania and zirconia (1.1 and 1.4 nm mean size), conduction electron spin resonance of the metal and paramagnetic F-centers (trapped electrons in oxygen vacancies) of the support were observed. Besides the influence of the surface geometry on the adsorption mode of the α,β-unsaturated aldehyde, the marked structure sensitivity of the catalytic properties with decreasing particle size is attributed to the electron-donating character of paramagnetic F-centers forming electron-rich gold particles as active sites. The effect of structural and electronic properties due to the quantum size effect of sufficiently small gold particles on the partial hydrogenation is demonstrated.

Introduction

The preferred hydrogenation of the carbonyl group of α,β-unsaturated aldehydes to yield allylic alcohols is an important step in the industrial synthesis of fine chemicals by selective catalytic hydrogenation of conjugated functional groups and has been attracting much interest for fundamental research in catalysis. The fundamental problem is that because of the stronger negative free reaction enthalpy of ∼35 kJ mol^{-1}, thermodynamics favors hydrogenation of the C=C over the C=O group. Furthermore, for kinetic reasons, the olefinic double bond is more reactive than the C=O group. Thus, as expected, conventional hydrogenation catalysts mainly provide saturated aldehyde or give rise to secondary hydrogenation into saturated alcohol. Therefore, it is desirable to find catalysts that allow control of the hydrogenation of the C=O group vs C=C group and, thus, of the intramolecular selectivity. Steric and electronic effects related to support material, attached ligands, and the structure and morphology of metal particle surfaces are among the most effective means of increasing selectivity to unsaturated alcohol.[1,2] In this way, in the meantime, selectively acting catalysts were developed particularly for hydrogenation in the liquid phase of cinnamaldehyde into cinnamyl alcohol (selectivity >96%) over Pt/Y zeolite[3] and from citral to geraniol/nerol (selectivity 96% at complete conversion) over an organometallic-derived $Rh[Sn-(n-C_4H_9)_2]SiO_2$ catalyst.[4] More intriguing is the selective hydrogenation of C_3 and C_4 α,β-unsaturated aldehydes such as acrolein and crotonaldehyde into the corresponding allylic alcohols. Recently, we have found excellent catalytic properties for supported silver nanoparticles in the hydrogenation of α,β-unsaturated aldehydes[1,5] in spite of being used in chemical industry almost exclusively to catalyze oxidation reactions. The selectivity to the unsaturated alcohol was entirely different from that of conventional hydrogenation catalysts comprising group 8−10 metals on nonreducible supports which do not produce unsaturated alcohols as a main product in gas-phase hydrogenations.[1,6−8] Because of the lack of space-filling substituents at the C=C group, acrolein is considered as the α,β-unsaturated aldehyde most difficultly hydrogenable to allylic

* Corresponding author: (e-mail) claus@chemie.tu-darmstadt.de.
† Darmstadt University of Technology.
‡ Institute for Applied Chemistry.
§ Max Planck Institute of Microstructure Physics.

(1) Claus, P. *Topics in Catalysis*; Somorjai, G. A., Thomas, J. M., Eds.; Special Issue *Fine Chemicals Catalysis, Part II*; Blackmond, D., Leitner, W., Eds.; Baltzer Science Publishers: Bussum, The Netherlands, 1998; Vol. 5, pp 51−62.
(2) Gallezot, P.; Richard, D. *Catal.-Rev.-Sci. Eng.* **1998**, *40*, 81−126.
(3) Gallezot, P.; Giroir-Fendler, A.; Richard, D. *Catal. Lett.* **1990**, *5*, 169−174.
(4) Didillon, B.; El-Mansour, A.; Candy, J. P.; Bournonville, J. P.; Basset, J. M. In *Stud. Surf. Sci. Catal. 59*; Guisnet, M., Barrault, J., Bouchule, C., Duprez, D., Perot, G., Maurel, R., Montassier, C., Eds.; Elsevier: Amsterdam, 1991; pp 137−143.
(5) (a) Claus, P. In *Catalysis of Organic Reactions*; Malz, R. E., Ed.; Chemical Industries Series 68; Marcel Dekker: New York, 1996; pp 419−422. (b) Claus, P.; Kraak, P.; Schödel, R. *Stud. Surf. Sci. Catal.* **1997**, *108*, 281−288.
(6) Claus, P.; Hönicke, D. In *Catalysis of Organic Reactions*; Scaros, M. G., Prunier, M. L., Eds.; Chemical Industries Series 62; Marcel Dekker: New York, 1995; pp 431−433.
(7) Berndt, H.; Mehner, H.; Claus, P. *Chem.-Ing.-Tech.* **1995**, *67*, 1332−1337.
(8) (a) Ponec, V. *Appl. Catal. A* **1997**, *149*, 27−48. (b) Marinelli, T. B. L. W.; Ponec, V. *J. Catal.* **1995**, *156*, 51−59. (c) Marinelli, T. B. L. W.; Naarburs, S.; Ponec, V. *J. Catal.* **1995**, *151*, 431−438.

10.1021/ja0012974 CCC: $19.00
Published on Web 11/03/2000

alcohol.[1,2,5a,8] Allyl alcohol is formed as the main product only when applying cadmium-containing catalysts.[9] However, in contrast to promoted catalysts with metals of the platinum group as the base metal,[8] by using Ag/SiO_2 in the gas-phase hydrogenation of acrolein at 453 K and 2 MPa, it was possible to achieve the formation of allyl alcohol with a selectivity of 50% at 56% conversion.[10]

This encouraged us to explore the potential of gold for the acrolein hydrogenation. For a long time, gold did not attract much attention in catalyst research and chemical engineering because it was catalytically much less active than the platinum-group metals due to its $5d^{10}$ electronic configuration. In the absence of a support material, on pure gold surfaces in general neither H_2, CO, nor O_2 is adsorbed, and hydrocarbons interact only weakly with gold surfaces.[11] The intrinsic inertness of gold may be reduced successfully by employing it highly dispersed on a suitable support. Under such conditions, reactions such as selective oxidation of hydrocarbons, low-temperature oxidation of CO, and reactions involving hydrogen are catalyzed by gold.[11] Downsizing the particle size dimensions, however, also affects their electronic character. For gold nanoparticles grown by vapor deposition in ultrahigh vacuum on single crystalline TiO_2 (110) surfaces, scanning tunneling spectroscopy revealed a band gap for particles smaller than 4 nm that increases in width, with further size reduction giving rise to nonmetallic character.[12] These results suggest that, if the gold-mediated hydrogenation depends on the metallic character, significant changes in catalytic properties should be observed with gold particles of sizes below 2−3 nm.[11]

Therefore, a thorough understanding of the unusual catalytic behavior of gold nanoparticles requires knowledge of their structural characteristics. One powerful method of catalyst characterization is transmission electron microscopy, including selected area electron diffraction, to study size distribution, crystal habit, surface structure, and surface composition of supported metal crystallites.[13,14] Electron paramagnetic resonance (EPR) is well suited to close the gap between nanoparticles around 1-nm size and clusters containing a few atoms only. The magnetic and electronic properties of such particles differ markedly from those of the bulk metal due to quantum size effects (QSE) first described by Kubo.[15] The essential issue of these phenomenona is that in nanosized particles the conduction electron band is not a continuum as in the bulk metal, but splits into discrete energy levels of spacing δ. This is, for example, the reason that, in heavy metal nanoparticles, conduction electron spin resonance (CESR) signals are frequently observed at higher temperature than in the bulk metal since with decreasing particle size, i.e., with increasing δ, the line width decrease due to longer relaxation times.[16] Recently, we have detected CESR signals in Ag particles of 1−3-nm diameter supported on TiO_2 (P25, Degussa).[17] The energy level spacing δ increases with decreasing particle volume according to eq 1,

$$\delta = (4E_F/3N) \approx 1/d^3 \quad (1)$$

where E_F is the Fermi energy of electrons, N is the number of conduction electrons, and d is the particle diameter.[16] According to Kawabata,[18] d is small enough to show QSE if the conditions $h\nu/\delta \gg 1$ and $h/\tau\delta \gg 1$ are fulfilled, where h is the Planck constant, ν is the microwave frequency, and τ is the spin relaxation time. Then the peak-to-peak line width ΔH_{pp} of CESR signals may be described by eq 2, where v_F is the Fermi velocity

$$\Delta H_{pp} = v_F(\Delta g_\infty)^2 h\nu\gamma_e^{-1}\delta^{-1}d^{-1} \approx d^2 \quad (2)$$

of electrons, Δg_∞ is the g-shift for the bulk metal ($\Delta g_\infty = g(\text{metal}) - g(\text{free electron})$), and γ_e is the electron magnetogyric ratio. By applying eqs 1 and 2, we estimated the diameter of Ag-on-titania particles which fairly well agreed with the transmission electron microscopy (TEM) size evaluation.[17]

For nanosized gold particles, only a few markedly different results with respect to CESR signals are published. While no CESR line was detected for Au particles (1.6−2.5 nm) dispersed in a lithium fluoride matrix,[19] a signal of 20-mT line width and 0.22−0.27 g-shift was observed for Au clusters of 3-nm mean diameter.[20] In contrast, a narrow CESR signal (line width 0.6−0.9 mT, $g = 2.0024$) at room temperature has been assigned to Au particles (2−8 nm) deposited on quartz.[21] With too small metal particles, discrimination between them and the support material by electron microscopy becomes difficult. Then, EPR is a sensitive technique for very small metal particles and clusters.

In the following, we will report in detail on the preparation and in-depth characterization of titania- and zirconia-supported gold nanoparticles by TEM/HREM, EPR, and UV/VIS-DRS measurements and their influence on activity and selectivity in the gas-phase hydrogenation of acrolein. The combination of these methods together with reaction experiments is a useful strategy to achieve a more detailed understanding of the influence of structural properties of very small gold nanoparticles on hydrogenation reactions. Since variations of the catalytic properties are expected in the 1−3-nm size range, we tried to determine whether there is a possible selectivity switching between hydrogenation of the C═C and C═O functional group and at which particle size this will occur.

Experimental Section

Supported Gold Catalysts. Three different gold-on-titania catalysts were prepared by the following methods: deposition−precipitation (DP), impregnation (I), and sol−gel techniques (SG). The support used for the DP and I methods was Degussa P25 titania (phase composition 65% anatase and 35% rutile,[22] specific surface area 50 m^2/g). The gold precursors for the DP and I methods were $HAuCl_4$ (Strem) and $AuCl_3$ (Aldrich), respectively. For the deposition−precipitation of $Au(OH)_3$ onto TiO_2, we started with the preparation of a suspension of 4.9 g of titania in 75 mL of distilled water followed by addition of ammonia (0.31 mL of a 4.98 N solution). Then, the gold precursor solution was prepared by dissolving 99 mg of $HAuCl_4$ in 10 mL of distilled water. Thereafter, the latter was added dropwise under vigorous stirring to the aqueous suspension of titania followed by addition of 4 mL of

(9) Claus, P.; Münzner, H.; Lucas, M. DE 195 33 578 C1, 1995.
(10) Claus, P.; Schrödter, K.; Hönicke, D.; Lücke, B. In *Selective Hydrogenation and Dehydrogenation*, DGMK Report 9305; Baerns, M., Weitkamp, J., Eds.; **1993**, 239−246.
(11) Bond, G.; Thompson, D. T. *Catal.-Rev.-Sci. Eng.* **1999**, *41*, 319−388.
(12) Valden, M.; Lai, X.; Goodman, D. W. *Science* **1998**, 281, 1647−1650.
(13) Rupprechter, G.; Hayek, K.; Hofmeister, H. *J. Catal.* **1998**, *173*, 409−422.
(14) Bernal, S.; Calvino, J. J.; Gatica, J. M.; Larese, C.; López-Cartes, C.; Pérez-Omil, J. A. *J. Catal.* **1997**, *169*, 510−515.
(15) Kubo, R. *J. Phys. Soc. Jpn.* **1962**, *71*, 975−986.
(16) Halperin, W. P. *Rev. Mod. Phys.* **1986**, *58*, 536−606.
(17) Claus, P.; Hofmeister, H.; Brückner, Lucas, M.; Mohr, C. *Proc. 98. Hauptversammlung der Deutschen Bunsen-Gesellschaft für Physikalische Chemie;*, 1999; p D71.
(18) Kawabata, A. *J. Phys. Soc. Jpn.* **1970**, *29*, 902−911.
(19) Sako, S. *J. Phys. Soc. Jpn.* **1990**, *59*, 1366−1371.
(20) Dupree, R.; Forwood, C. T.; Smith, M. J. A. *Phys. Status Solidi* **1967**, *24*, 525−530.
(21) Monot, R.; Châtelein, A.; Borel, J.-P. *Phys. Lett.* **1971**, *34A*, 57−58.
(22) Claus, P.; Schimpf, S.; Schödel, R.; Kraak, P.; Mörke, W.; Hönicke, D. *Appl. Catal.* **1997**, *165*, 429−441.

Table 1. Designation and Texture Properties of the Titania- and Zirconia-Supported Gold Catalysts Used in This Study

catalyst designation	preparation method	gold content (wt %)	surface area (m^2/g)	pore vol (mL/g)
Au/TiO_2-DP	deposition−precipitation	1.7	42	0.35
Au/TiO_2-I	impregnation	2.9	42	0.38
Au/TiO_2-SG	sol−gel	4.8	117	0.17
Au/ZrO_2-F	coprecipitation	1.0	151	0.37

ammonia. After stirring for 6 h and aging for 3 h, the slurry was filtered and washed with distilled water until it was chloride-free (proved by addition of silver nitrate). Drying (373 K, 12 h), calcination in flowing air (573 K) for 8 h, and reduction in flowing hydrogen at 573 K for 3 h gave the final catalyst, Au/TiO_2-DP.

In the case of the impregnated catalyst, Au/TiO_2-I, the gold precursor solution consisted of $AuCl_3$ dissolved in distilled water (0.25 mol L^{-1}) which was added dropwise to the titania (0.6 mL/g of TiO_2). For this catalyst, the same treatment conditions in drying, calcination, and reduction as described above for Au/TiO_2-DP were applied.

The sol−gel-derived titania-supported gold catalyst, Au/TiO_2-SG, was prepared by using tetrabutoxytitanium(IV) (TBOT, purchased from Aldrich), gold acetate (99.9%, from Alfa), methanol (HPLC grade), and distilled water as starting components in the following procedure. At first, according to Schneider et al.,[23] a solution of TBOT (32 g) in methanol (120 mL) was mixed with a second solution consisting of 30 mL of methanol, 6.78 mL of water, and 0.5 mL of HNO_3 (65 wt %). At room temperature and under vigorous stirring, a lucid gel was obtained within 20−30 min. Then, after aging for 2 h, the titania gel was redispersed in 250 mL of methanol to give a clear solution (titania precursor sol). Gold acetate (770 mg) was dissolved in a mixture of 125 mL of methanol and 12.6 of water and sonicated (0.5 W cm^{-2}, 35 kHz) for 5 min (Au precursor solution). By sonochemical preparation, stable colloidal metal dispersions and nanoparticles with narrow particle size distributions have been formed.[24] Subsequently, the Au precursor solution was added dropwise to the titania precursor sol, and this mixture was vigorously stirred for 2 h. To evaporate the solvent prior to drying, the viscous solution was stirred in a rotary evaporator at 323 K until gelation occurred. The resulting solid was deep purple. It was dried at 453 K for 12 h in an oven, followed by calcination in flowing air (90 mL min^{-1}) at 673 K (4 h) and reduction in flowing hydrogen (90 mL min^{-1}) at 723 K (3 h) to give the catalyst Au/TiO_2-SG. For comparison, pure sol−gel-derived TiO_2 was prepared by the same procedure but without introducing the gold precursor solution.

A zirconia-supported gold catalyst, noted as Au/ZrO_2−F, was prepared by coprecipitation. Two solutions were prepared. The first solution consisted of 141.1 mg of $HAuCl_4$ dissolved in 10 mL of H_2O and the second of 10 g of $ZrOCl_2 \cdot 8H_2O$ (99.99 wt %, from Aldrich) in 35 mL of H_2O. The latter was added into a beaker to the aqueous solution of $HAuCl_4$ followed by adding 14.2 mL of ammonia (4.98 N) under stirring. The resulting coprecipitate was filtered, washed with water, and then dried at 393 K for 8 h. Calcination in flowing air at 573 K for 8 h and reduction in flowing hydrogen at 573 K for 5 h gave the final catalyst, Au/ZrO_2-F.

The gold contents of the catalysts were determined by atomic emission spectroscopy with inductively coupled plasma (AES-ICP, Perkin-Elmer Optima 3000XL) after dissolving the materials in a mixture of HF/HNO_3 by means of a MDS-2000 microwave unit (CEM).

The designations of the supported gold catalysts used in this study and their metal contents are compiled in Table 1.

Electron Microscopy (TEM, HREM). Qualitative and quantitative characterization of the catalysts were carried out using a JEM 100C operating at 100 kV for TEM in bright-field and dark-field modes. Crystallinity and crystal structure of the samples were evaluated from selected area electron diffraction (SAED) patterns as well as by high-resolution electron microscopy (HREM) done at a JEM 4000EX operating at 400 kV. For electron microscopy examination, the catalyst samples were dissolved in 2-propanol, dispersed carefully in an ultrasonic bath, and then deposited on carbon coated copper grids. Image processing for, for example, contrast enhancement and image evaluation, was done at digitized electron micrographs by means of the programs Digital Micrograph (Gatan) and NIH Image.[25]

Electron Paramagnetic Resonance (EPR). EPR spectra of samples Au/TiO_2-SG, Au/TiO_2-DP, Au/TiO_2-I, Au/ZrO_2-F, and TiO_2 were recorded with the cw spectrometer Elexsys 500-10/12 (Bruker) in X-band ($\nu = 9.515$ GHz) at 77 and 293 K using a finger dewar. The magnetic field was measured with reference to a standard of 2,2-diphenyl-1-picrylhydrazyl hydrate (DPPH). Reduction of the catalysts was performed in flowing hydrogen (45 mL min^{-1}) at 723 K (samples Au/TiO_2-SG and TiO_2) and 573 (sample Au/ZrO_2), respectively, with an EPR flow cell consisting of two coaxial tubes similar to that described by Mesaros and Dybowski.[26] EPR spectra were recorded after treatment in H_2 without contact to ambient atmosphere.

UV/VIS-DRS. UV/VIS-DRS measurements were performed by a Cary 400 spectrometer (Varian) equipped with a praying mantis diffuse reflectance accessory (Harrick). All samples were diluted with $BaSO_4$ white standard (Merck) in 1:50 ratio.

Selective Hydrogenation of Acrolein. Gas-phase hydrogenation of acrolein (AC, purchased from Aldrich) was carried out in a computer controlled fixed-bed microreactor system which has been described in detail elsewhere.[27] This equipment allows the performance of high-pressure gas-phase hydrogenations of unsaturated organic compounds, which are usually liquids with low vapor pressures at standard conditions (STP). The reactor effluents were on-line analyzed by an HP 5890 gas chromatograph, equipped with a flame ionization detector and a 30-m J&W DB-WAX capillary column. The gold catalysts were reduced in situ at the conditions described above. The reaction conditions of the acrolein hydrogenation were as follows: temperature range 453 K $\leq T \leq$ 593 K, total pressure $p = 2$ MPa, molar ratio $H_2/AC = 20$, reciprocal space time $W/F^{o}_{Ac} = 15.3$ g_{cat} h mol^{-1}, where W is the weight of catalyst (0.23 g; particle size 0.2−0.5 mm) and F is the molar flow of acrolein. Temperatures in the range of 513−553 K were required for zirconia-supported gold catalysts to be active, and conversion data up to 10% were obtained. Using Au/TiO_2 catalysts, acrolein hydrogenation to allyl alcohol and propanal started at lower temperatures around 473 K. For the purpose of comparison, the catalytic data are reported at 513 K, which is close to a common reaction temperature for all catalytic runs. Over the titania-based catalysts, increased formation of 1-propanol due to consecutive hydrogenation of propanal and allyl alcohol was observed above 553 K. Moreover, the extent of C_2 and C_3 hydrocarbon formation also increased at higher temperatures because of the increased extent of side reactions (decarbonylation of acrolein and propanal, dehydratization of allyl alcohol). All the gold catalysts exhibited good activity maintenance during the time on stream (catalytic runs over 3 h). Minimal activity loss was only observed during the first 10 min in the case of Au/TiO_2 catalysts. This could be due to the formation of acrylic acid and formyldihydropyran, which were detected as byproducts. At 553 K, they were formed with a maximum selectivity of 8%. In contrast to that, acrolein hydrogenation at temperatures between 513 and 553 K over Au/ZrO_2 catalysts gave allyl alcohol and propanal as main products beside traces of 1-propanol and hydrocarbons. Note, that all given catalytic data (specific activities, selectivities) are based on steady-state behavior of the catalysts. The selectivities of reaction products were calculated from moles of product formed per moles of acrolein converted, and the catalyst activities were expressed as specific activities (on a gram of gold basis).

(23) Schneider, M.; Duff, D. G.; Mallat, T.; Wildberger, M.; Baiker, A. *J. Catal.* **1994**, *147*, 500−514.

(24) (a) Okitsu, K.; Mizukoshi, Y.; Bandow, H.; Maeda, Y.; Yamamoto, T.; Nagata, Y. *Ultrason. Sonochem.* **1996**, *3*, 249−251. (b) Okitsu, K.; Nagaoka, S.; Tanabe, S.; Matsumoto, H.; Mizukoshi, Y.; Nagata, Y. *Chem. Lett.* **1999**, 271−272. (c) Salkar, R. A.; Jeevavandam, P.; Aruna, S. T.; Koltypin, Y.; Gedanken, A. *J. Mater. Sci.* **1999**, *9*, 1333−1335.

(25) Rasband, W. *NIH Image*; public domain software, U.S. National Institute of Health, FTP: zippy.nimh.nih.gov.

(26) Mesaros, D. V.; Dybowski, C. *Appl. Spectrosc.* **1987**, *41*, 610−612.

(27) Lucas, M.; Claus, P. *Chem.-Ing.-Tech.* **1995**, *67*, 773−777.

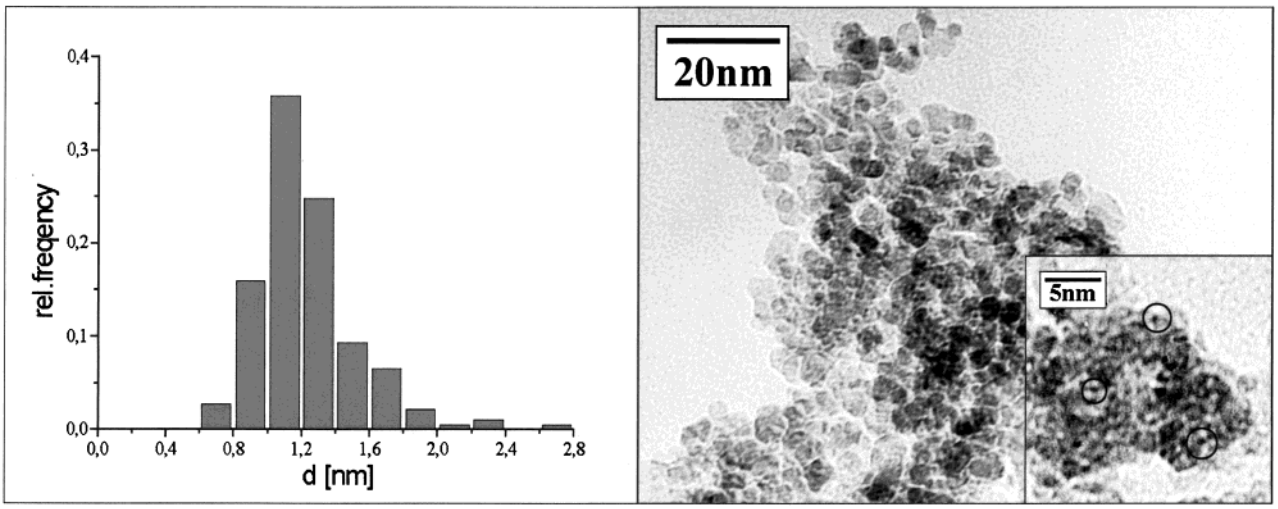

Figure 1. Size distribution (left) and CTEM overview (right) of the catalyst Au/TiO_2-SG.

Table 2. Gold Particle Sizes and Degree of Dispersion Estimated by TEM Analysis

catalyst	$\bar{d}_{Au}$[a] (nm)	msd[b] (nm)	D_{Au}[c]
Au/TiO_2-DP	5.3	0.3	0.36
Au/TiO_2-I	2.0	0.4	0.47
Au/TiO_2-SG	1.1	0.2	0.78
Au/ZrO_2-F	1.4	0.3	0.63

[a] Mean diameter of log-normal distribution. [b] Mean square displacement. [c] Estimated from the ratio of the number of surface atoms to the total number of atoms as calculated for the mean particle size by assuming closed-shell particles of sperical shape.

Results

Particle Size Characteristics. Before electron microscopy investigation, all samples were subjected to a reduction treatment in hydrogen flow. For visual comparison of the four different catalysts studied, TEM overviews together with the corresponding size distribution are given in Figures 1−4. From these figures, it may be recognized that highly dispersed, nanometer-sized gold particles in the range of 1−6 nm with mostly narrow size distributions have been produced. The characteristics of these distributions, i.e., the mean particle diameter, $\bar{d}_{Au}$, together with the mean square displacement, msd (summarized in Table 2), may serve for a quantitative comparison of the catalysts. For every sample, using a χ^2 test, we determined whether a monomodal standard distribution or a log-normal distribution is valid. We found that the latter describes best all measured values. The corresponding degree of gold dispersion was roughly estimated from the ratio of the number of surface atoms to the total number of atoms calculated from the mean particle size by assuming closed-shell particles of nearly spherical shape.[28] By comparing the TEM analyses for the titania-supported gold catalysts, an increase of mean particle size and msd increase following the sequence sol−gel technique, impregnation and deposition-precipitation is found. In Au/TiO_2-SG, we observed extremely small, nearly spherical particles. These gold particles exhibit a very narrow size distribution (Figure 1) and a very small mean particle size, $\bar{d}_{Au} = 1.1 \pm 0.2$ nm, i.e., an exceedingly high degree of gold dispersion ($D_{Au} = 0.78$). Thus, by using our simple sol−gel technique described in the Experimental Section, downsizing to give nanoparticles of mean particle sizes down to 1 nm is possible without using additional organic compounds as stabilizers (e.g., surfactants, polymers, ligands).[29] Moreover, this size distribution is much narrower as compared to other routes of synthesis of supported nanosized gold clusters as, for example, through inverse micelle/sol−gel synthesis[30] and Au−phosphine clusters.[31] Due to the sol−gel synthesis, most of the gold particles of the Au/TiO_2-SG sample are embedded in the TiO_2 network, which makes electron microscopy characterization somewhat difficult because of their small sizes and the contrast features (eigen contrast) of this highly nonplanar and nonuniform support material.

Au/TiO_2-I exhibits a broader size distribution and a larger mean size, $\bar{d}_{Au} = 2.0 \pm 0.4$ nm (Figure 2). Nevertheless, a certain amount of particles smaller than ~1 nm, being "invisible" for electron microscopy, may be present and change slightly the actual mean size in this and all other samples. As revealed by dark-field imaging, the gold particles are situated at the surfaces of TiO_2 grains. HREM revealed that the smallest gold particles were mostly single crystalline, but the larger ones partly exhibited some defect structures. Gold particles of Au/TiO_2-DP (Figure 3) are the largest among the titania-supported ones, $\bar{d}_{Au} = 5.3 \pm 0.3$ nm. They showed mostly octahedral facets and also distinct single crystalline electron diffraction patterns (SAED). Mean particle sizes smaller than 5 nm are usually achieved during deposition−precipitation by pH above 6 where the main gold species in solution is transformed from $AuCl_4$ to $Au(OH)_nCl_{4-n}$ ($n = 1-3$) as shown for calcined Au/TiO_2 catalysts.[32] The gold particle size of the catalyst Au/ZrO_2-F (Figure 4) is found to be $\bar{d}_{Au} = 1.4 \pm 0.3$ nm, which is similar to the 1.1 ± 0.2 nm size of the sol−gel-derived gold-on-titania catalyst. These gold particles are in good approximation spherical and have a larger amount of lattice defects. The results presented above show that, besides depending on synthesis and processing, the size and morphology of Au nanoparticles distintly are governed by the choice of a suitable oxide support.

Quantum Size Effects. The EPR spectrum of sample Au/TiO_2-SG recorded before reduction in hydrogen flow (Figure

(28) Montejano-Carrizales, J. M.; Aguilera-Granja, F.; Moran-Lopez, J. L. *Nanostruct. Mater.* **1997**, *8*, 269−287.

(29) (a) Bradley, J. S. The Chemistry of Transition Metal Colloids In *Cluster and Colloids: From Theory to Applications*; Schmid, G., Ed.; VCH: Weinheim 1994; pp 459−536. (b) Brown, L. O.; Hutchinson, J. E. *J. Am. Chem. Soc.* **1999**, *121*, 882−883. (c) Bönnemann, H.; Wittholt, W.; Jentsch, J. D.; Schulze Tilling, A. *New J. Chem.* **1998**, 713−717. (d) Vossmeyer, Th.; Delonno, E.; Heath, J. R. *Angew. Chem.* **1997**, *109*, 1123−1124. (e) Ohara, P. C.; Heath, J. R.; Gelbart, W. *Angew. Chem.* **1997**, *109*, 1120−1122.

(30) Martino, A., Yamanaka, S. A., Kawola, J. S., Loy, D. A. *Chem. Mater.* **1997**, *9*, 423−429.

(31) Kozlov, A. I.; Kozlova, A. P.; Liu, H.; Iwasawa, Y. *Appl. Catal.* **1999**, *182*, 9−28.

(32) Haruta, M. *Catal. Today* **1997**, *36*, 153−166.

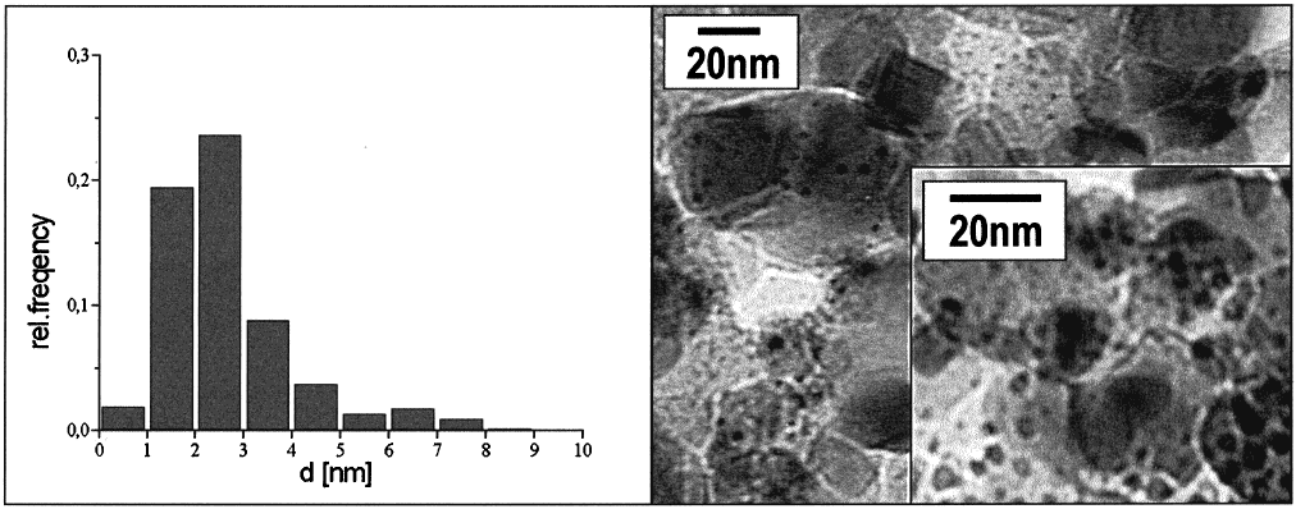

Figure 2. Size distribution (left) and CTEM overview (right) of the catalyst Au/TiO_2-I.

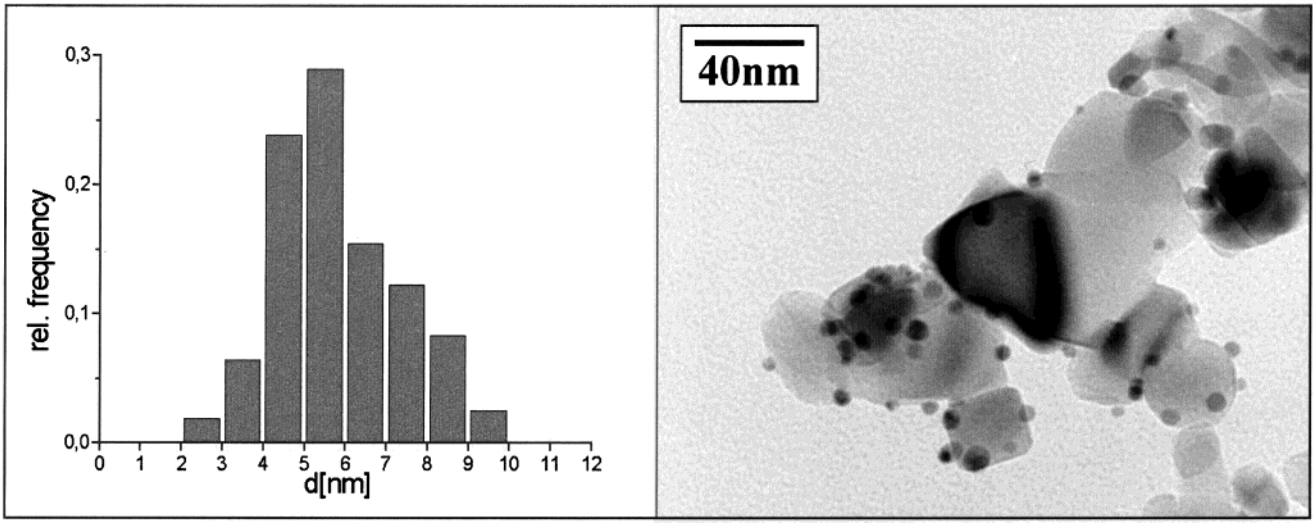

Figure 3. Size distribution (left) and CTEM overview (right) of the catalyst Au/TiO_2-DP.

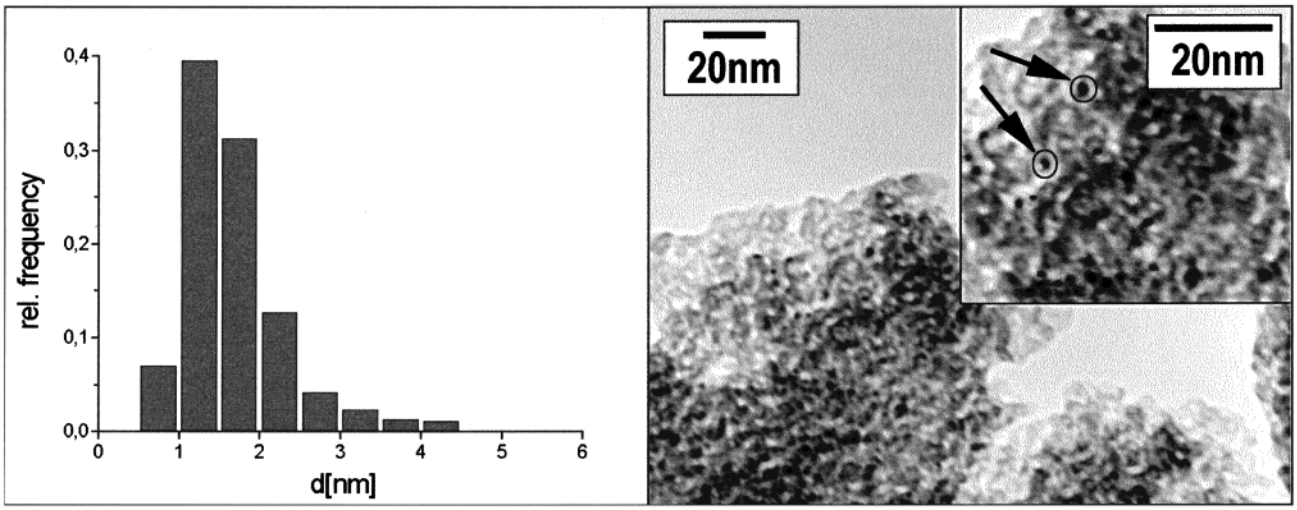

Figure 4. Size distribution (left) and CTEM overview (right) of the catalyst Au/ZrO_2-F.

5a) contains a hyperfine quartet ($A = 4.5$ mT) which may be due to the $g_\perp$ part of Au^{2+} ions (^{197}Au: $I = {}^3/_2$, 100% natural abundance). This is in agreement with data measured for Au^{2+} ions in gold fluoride.[33] The quartet is superimposed on a narrow singlet close to the free electron g-value. Upon reduction in hydrogen at 723 K, the hyperfine quartet vanishes since Au^{2+} ions are reduced to elementary gold (Figure 5b). Simultaneously, a strong signal at $g = 1.936$ assigned to Ti^{3+} [22] appears that indicates a marked reduction of the support. When the reduced sample is stored in ambient atmosphere, the Ti^{3+} signal vanishes

(33) Bork, M.; Hoppe, R.; Hofstaetter, A.; Scharmann, A.; Wagner, F. E. *Z. Anorg. Allg. Chem.* **1996**, *622*, 1721−1728.

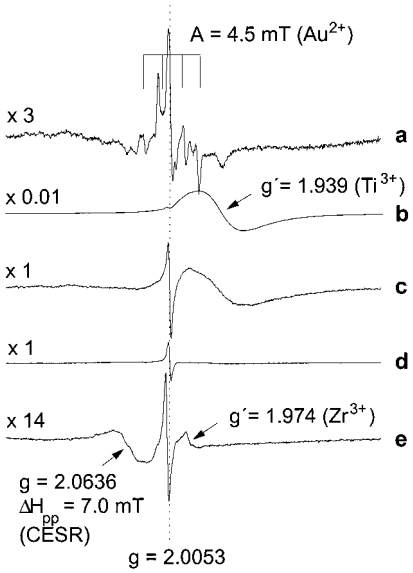

Figure 5. EPR spectra at 77 K (300 mT < B_0 < 390 mT) of Au/TiO_2-SG after drying at 453 K (a), after reduction at 723 K in H_2 flow (b), after 18-h exposure to ambient atmosphere (c), after exposure to air for several weeks (d), and of Au/ZrO_2-F after reduction at 573 K in H_2 flow and exposure to ambient atmosphere for several weeks (e).

again with time due to reoxidation; however, the narrow singlet at $g = 2.0053$ is still present (Figure 5c,d). While the latter can also be detected at room temperature, the Ti^{3+} signal can only be seen at 77 K due to the short relaxation time. In the case of samples Au/TiO_2-I and Au/TiO_2-DP (not shown here), no signal is visible in the room-temperature spectra. The only EPR signal detectable in the spectra of these samples is that of Ti^{3+} at 77 K after reduction.

Now the question arises whether the singlet at $g = 2.0053$ in Figure 5a−d is due to CESR of small Au particles as assigned by Monot et al.[21] According to Kawabata, the g-shift of a CESR signal is determined by $\Delta g = \Delta g_\infty - h/2\pi\delta\tau$.[18] For particles small enough to exhibit QSE, the last term tends to zero since $\delta \gg h\nu$ and $\delta \gg h/\tau$. Hence, $\Delta g = \Delta g_\infty$ should be observed. On the other hand, the magnitude of Δg_∞ increases with the spin−orbit interaction.[16] This contribution becomes important for the heavier metals so that the g-shift of QSE particles increases too. For silver particles, Δg-values of 0.0077, 0.0317,[34] and 0.0117 [17] have been observed. The g-shift of gold particles is expected to be at least in the same order of magnitude or even larger. Thus, it is rather unlikely, that the signal at $g = 2.0053$ in Figure 5 and also the signal observed by Monot et al.[21] are due to CESR of nanosized Au particles.

To facilitate reliable assignment of the signals, the sol−gel -derived TiO_2 support prepared by the same procedure but without addition of gold has been studied by EPR in the same way (Figure 6). The spectra at 77 K indicate a redox behavior of the titanium ions similar to that observed in sample Au/TiO_2-SG. After reduction, a strong singlet is seen at 293 K, the line width and g-value of which are almost equal to those occurring in sample Au/TiO_2-SG (Figure 5a−d). That means position and shape of this line are characteristic for paramagnetic defects, namely, F-centers (single electrons trapped in anion vacancies).[35] This assignment is supported by the fact that the TiO_2 sample is black after reduction. It is well known that F-centers in ionic crystals give rise to deep colors. For example, ZrO_2 nanopowder

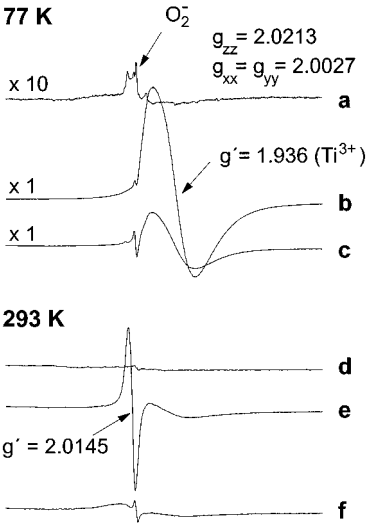

Figure 6. EPR spectra at 77 and 293 K (300 mT < B_0 < 390 mT) of the sol−gel-derived support TiO_2: (a, d) as-received; (b, e) after reduction at 723 K in flowing H_2; (c, f) reduced sample after 18-h storage in ambient atmosphere.

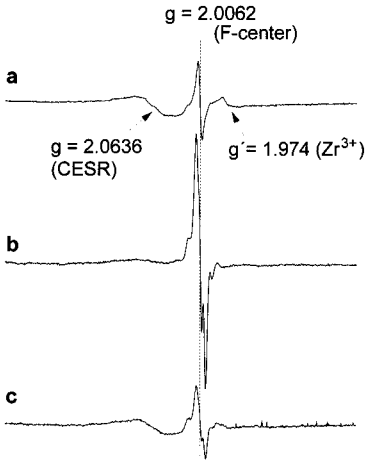

Figure 7. EPR spectra at 77 K of sample Au/ZrO_2-F: (a) as-received (dried at 393 K, calcined in flowing air at 573 K, reduced in flowing H_2 at 573 K, exposure to air); (b) after in situ reduction at 673 K in flowing H_2; (c) reduced sample after 20-h storage in ambient atmosphere.

with a high concentration of F-centers was found to be brown.[35] During exposure to air, the color of reduced TiO_2 turns to white again, the defect signal at 293 K decreases markedly, and the characteristic signal for O_2^- radicals appears at 77 K (Figure 6c,f), the formation of which can be explained by reaction of molecular oxygen with the F-centers. On comparing the EPR results of Au/TiO_2-SG and pure TiO_2, it is quite evident that the singlet at $g' = 2.0053$ in the former is due to F-centers formed by reduction of the TiO_2 support and does *not* originate from CESR of small Au particles.

The EPR spectrum of Au/ZrO_2-F contains a similar narrow singlet near the free electron g-value (Figure 5e) although its intensity is markedly lower than in Au/TiO_2-SG. It is assigned to F-centers in ZrO_2.[35] Additionally, signals at $g' = 1.974$ for Zr^{3+} and at $g' = 2.0636$ occur. The latter vanishes almost completely after repeated treatment in flowing hydrogen at 673 K for 3 h (Figure 7b), while the F-center signal as it was observed also vanishes after reduction of TiO_2. As in TiO_2, upon exposure to air, the concentration of F-centers decreases while

(34) Hughes, A. E.; Jain, S. C. *Adv. Phys.* **1979**, *28*, 717−828.
(35) Liu, H.; Feng, L.; Zhang, X.; Xue, Q. *J. Phys. Chem.* **1995**, *99*, 9, 332−334.

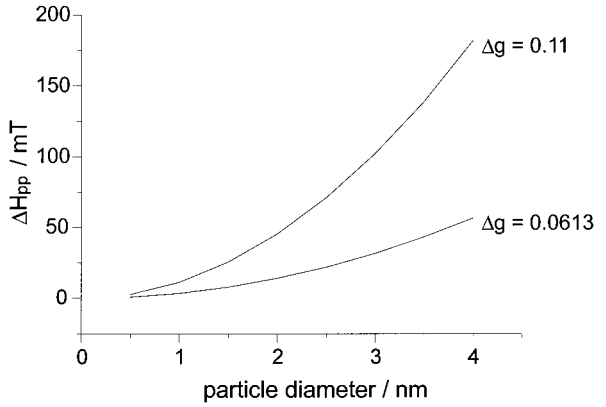

Figure 8. Relation between the peak-to-peak line width of the CESR signal and the particle diameter calculated by eq 3 using $\Delta g = 0.0613$ of sample Au/ZrO_2-F and the bulk metal g-shift $\Delta g_\infty = 0.11$ [25], respectively.

the line at $g' = 2.0636$ reappears (Figure 7c). The large g-shift suggests an assignment of this signal to CESR of small Au particles.

As mentioned above, the diameter of QSE particles is related to the peak-to-peak line width of the respective CESR signal, using eqs 1 and 2. With the density of gold ($\rho_{Au} = 197.2$ g mol^{-1}) and assuming a spherical particle shape, eq 1 yields $\delta = 3.82 \times 10^{-47}$ d^{-3}. Inserting this value in eq 2 and taking $\nu_F = 10^6$ m s^{-1}, $\gamma_e = 1.76 \cdot 10^{11}$ s^{-1} T^{-1}, $E_F = 8.8 \times 10^{-19}$ J, and $h\nu = 6.3 \cdot 10^{-24}$ J, the relation between the particle diameter and the peak-to-peak line width becomes

$$d^2\,[\mathrm{m}] = 1.066 \times 10^{-18} \Delta H_{pp}\,(\mathrm{T})(\Delta g)^{-2} \qquad (3)$$

With the experimental values of sample Au/ZrO_2-F ($\Delta g = 0.0613$, $\Delta H_{pp} = 6.9$ mT), a particle diameter of $d_{Au} = 1.4$ nm is calculated, which is exactly the value obtained by TEM measurements (see Table 2). This result, too, indicates that the assignment of the signal to CESR of Au particles is reliable.

From Figure 8 it can be seen that the peak-to-peak line width increases rapidly with the particle diameter. Using $\Delta g = 0.0613$, a line width of 38.4 mT would result for Au/TiO_2-I (TEM-derived $d_{Au} = 2.0$ nm) and of 118.6 mT for Au/TiO_2-DP ($d_{Au} = 5.3$ nm). Both values are far beyond detection of low-intensity signals. The line broadening would be even more pronounced for higher g-shifts when approaching the bulk metal value of $\Delta g_\infty = 0.11$ (Figure 8).[36] Thus, it is easily understood why no CESR signals are observed in the spectra of the two latter samples. In the case of Au/TiO_2-SG ($d_{Au} = 1.1$ nm) for which such a signal should be expected, dipolar interaction of the Au particles with the F-centers in the support may broaden the line and prevent detection. In fact, such a process is observed, too, for the CESR signal of sample Au/ZrO_2-F after reduction when the F-center concentration is high (Figure 7b). Interestingly, it was shown that already calcined ZrO_2 has two types of similar EPR signals which may be assigned to bulk Zr^{3+} ions and surface-related F-centers[35] comparable to that in Figure 7a.

Because of the distinct surface plasmon resonances of small noble metal particles, optical absorption spectroscopy is well suited to complete the in-depth structural characterization of our metal/oxide nanoparticulate composites. The relative ease of recording such spectra must be faced with the difficulties of interpreting the rather complex results. In the UV/visible spectra of Au/TiO_2-SG, Au/TiO_2-DP, and Au/ZrO_2-F (Figure 9), the typical plasmon band of small Au particles between 500 and

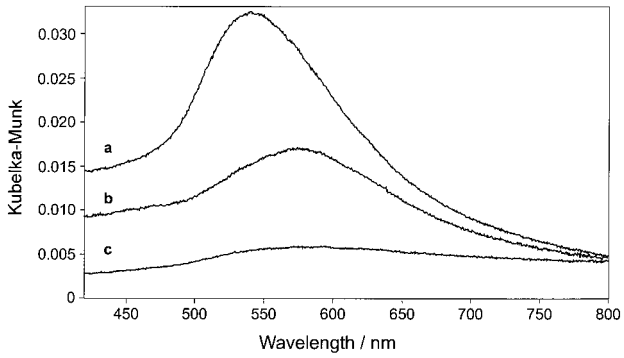

Figure 9. UV/visible-diffuse reflectance spectra of the reduced samples: (a) Au/TiO_2-DP, (b) Au/TiO_2-SG, and (c) Au/ZrO_2-F.

600 nm is evident.[37,38] For the titania-supported gold catalysts prepared by deposition−precipitation and sol−gel technique, the spectra in Figure 9 reveal the expected trend that the bandwidth decreases from full with at half-maximum (fwhm) = 136 nm (curve b) to fwhm = 115 nm (curve a) with the particle size increasing from $d_{Au} = 1.1$ nm to $d_{Au} = 5.3$ nm, i.e., $d_{(Au/TiO2-SG)} < d_{(Au/TiO2-DP)}$. The mean particle diameter is related to the peak position and full width at half-height of the plasmon band.[39] This relation, however, is not only influenced by the width and shape of the particle size distribution but also by the dielectric function of the supporting or surrounding medium as well as possible particle interactions deviating from the single-particle assumption of Mie's theory.[40] A careful interpretation of the spectra obtained would require extensive calculations according to appropriate models, which is beyond the scope of the present paper. In the context of these considerations, it may be understood that Au/ZrO_2-F exhibits a greater fwhm (163 nm) than Au/TiO_2-SG although the latter is characterized by the highest degree of gold dispersion (Table 2). The described nanoparticle characteristics, however, are thought to play an important role in determining the catalytic behavior of the gold catalysts that will be treated in the following section.

Particle-Mediated Hydrogenation of Acrolein over Nanosized Gold on TiO_2 and ZrO_2. As shown in Figure 10, the hydrogenation of acrolein over the titania-supported catalysts Au/TiO_2-DP and Au/TiO_2-I at 453 K and 2 MPa gave, at acrolein conversion of <10%, the desired allyl alcohol with a selectivity of 41 and 43%, respectively, as a consequence of the hydrogenation of the C=O group. Note, that this steady-state level of selectivity is up to 1 order of magnitude higher than in the case of supported group 8−10 metals used for the hydrogenation of acrolein.[8,41] The competitive hydrogenation of the C=C bond of acrolein to give propanal mainly accounts for the difference to 100% selectivity, whereas the formation of further possible reaction products (propanol by consecutive hydrogenation, hydrocarbons by decarbonylation of aldehydes, acrylic acid by oxygen transfer from the support, formyldihydropyran by acrolein dimerization) contributes only to a much

(36) Monod, P.; Janossy, A. *Low Temp. Phys.* **1977**, *26*, 311−316.

(37) Logunov, S. L.; Ahmadi, T. S.; El-Sayed, M. A.; Khoury, J. T.; Whetten, R. L. *J. Phys. Chem. B* **1997**, *101*, 3713−3719.

(38) (a) Kreibig, U.; Genzel, L. *Surf. Sci.* **1985**, *156*, 678−700. (b) Charle, K.-H.; König, L.; Nepijko, S.; Rabin, I.; Schulze, W. *Cryst. Res. Technol.* **1998**, *33*, 1085−1096.

(39) Berg, K.-J.; Berger, A.; Hofmeister, H. *Z. Phys. D* **1991**, *20*, 309−312.

(40) (a) Schönauer, D.; Lauer, H.; Kreibig, U. *Z. Phys. D* **1991**, *20*, 301−304. (b) Dusemund, B.; Hoffmann, A.; T. Salzmann, T.; Kreibig, U.; Schmid, G. *Z. Phys. D* **1991**, *20*, 305−308. (c) Berger, A.; Berg, K.-J.; Hofmeister, H. *Z. Phys. D* **1991**, *20*, 313−316.

(41) Mohr, C.; Hofmeister, H.; Lucas, M.; Claus, P. *Chem.-Ing.-Tech.* **1999**, *71*, 869−873.

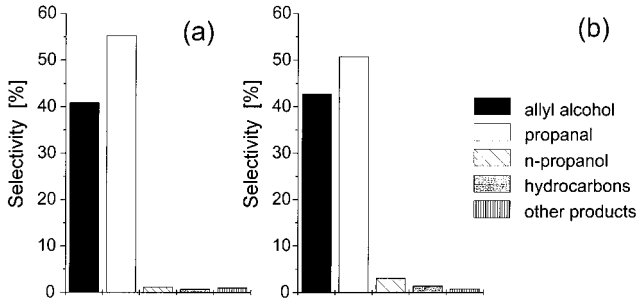

Figure 10. Selectivities to reaction products in the gas-phase hydrogenation of acrolein over (a) Au/TiO_2-DP and (b) Au/TiO_2-I at T = 453 K, p_{total} = 2 MPa, H_2/acrolein = 20, and W/F^o_{Ac} = 15.3 g h mol^{-1} (conversion < 10%).

less extent to the product composition. Moreover, keeping in mind the size of the gold particles in both catalysts, Au/TiO_2-DP (d_{Au} = 5.3 nm) and Au/TiO_2-I (d_{Au} = 2 nm), it is obvious, that the selectivity is nearly independent of the particle size. Thus, the hydrogenation of acrolein over Au/TiO_2 catalysts appears to be structure-insensitive for sizes above 2 nm, although a particular catalytic system can exhibit structure sensitivity in only a small range of the particle size.[42] It is noteworthy to mention that at 453 K the other two gold catalysts of the present study, Au/TiO_2-SG and Au/ZrO_2-F, showed no activity so that higher temperatures (513−593 K) had to be applied. Therefore, in Table 3, the catalytic properties in terms of activity, apparent activation energy, and selectivity data of all catalysts are compared at 513 K. Note that, within the whole temperature range, the selectivity to the reaction products was independent of acrolein conversion for Au/TiO_2-SG and Au/ZrO_2-F whereas with the catalysts Au/TiO_2-DP and Au/TiO_2-I the selectivity to allyl alcohol was somewhat lower due to secondary reactions (formation of propanol and hydrocarbons). However, again the selectivity (25%), catalyst activity, and also the apparent activation energy did not depend on the gold particle size (see Table 3). Interestingly, with further lowering of the gold particle size to 1.4 (Au/ZrO_2-F) and 1.1 nm (Au/TiO_2-SG), a drastic decrease of the catalytic activity was observed by up to 2 orders of magnitude (Table 3). Likewise, the apparent activation energy and the selectivity to allyl alcohol were diminished: With the 1.4-nm Au particles of the catalyst Au/ZrO_2-F, the lowest apparent activation energy was found. In line with the antipathetic structure sensitivity are the findings for a zirconia-supported gold catalyst prepared by the deposition−precipitation technique[41] (Au/ZrO_2-DP; see Table 3): Although a comparison is somewhat difficult because of its bimodal particle size distribution, it is obvious that gold particles above 2 nm in size yielded a considerably higher selectivity to allyl alcohol (42%). However, the low activity of the sol−gel-derived catalyst could also be due to particles, either surrounded by titania or partially buried within the support framework, leading to a reduction of the accessible gold surface area. There may be also contributions from covering the gold by residual organic material or even by modification of the electronic properties of metal particles through their coordination to titania.

Discussion

In a first approximation, the pronounced change of the catalytic behavior of TiO_2- and ZrO_2-supported gold particles with changes of the particle size can be satisfactorily accounted for by steric constraints on the metal surface: If hydrogenation of the C═O group of the α,β-unsaturated aldehyde is favored by face atoms, most likely the increased fraction of dense (111) planes of the larger gold particles will give higher formation rates of the allylic alcohol than low-coordinated atoms of smaller sized particles. In terms of reaction mechanism, this means that the C═O group is preferentially activated on the closed-packed structure of the (111) surface whereas sites of low coordination, mostly present on small particles as corners and edges, strongly favor the activation of the C═C group. Interestingly, this unusual catalytic behavior of gold catalysts is comparable with the structure sensitivity observed in our studies over titania-supported nanosized silver particles used for the selective hydrogenation of crotonaldehyde,[43] where the ultradispersed 1.4-nm Ag particles gave both a lower activity and selectivity to the unsaturated alcohol than the 2.8-nm Ag particles. Evidence for the antipathetic structure sensitivity emerges also from studies with platinum catalysts where a marked increase of selectivity toward the unsaturated alcohol with increasing fraction of Pt(111) surfaces has been observed in the hydrogenation of crotonaldehyde.[44]

However, in sufficiently small particles, changes of the surface coordination are linked to changes in electronic properties. Hence, in addition to the influence of the surface geometry determining the adsorption mode of the α,β-unsaturated aldehyde,[43−45] unusual electronic properties of nanosized gold should be taken into consideration to understand the significant changes of the hydrogenation behavior observed by downsizing the particles, i.e., when particle sizes of <2 nm gave 1−2 orders of magnitude lower catalytic activities and hydrogenate preferrably the olefinic double bond instead of the carbonyl group. It is likely that a marked change in the electronic character of nanosized gold particles in the 1−2-nm range may indicate a transition to the nonmetallic phase and that the structure sensitivity originates from a quantum-size effect. On the other hand, gold particles larger than 2−3 nm are certainly metallic in character and activate the C═O group to produce allyl alcohol with significantly higher selectivity at increased activity. Indeed, as shown by Valden et al.,[12] who prepared Au/TiO_2 model catalysts by vapor deposition on single crystalline titania TiO_2 surfaces, a metal-to-nonmetal transition occurs as the gold cluster size decreased below 300 atoms per cluster (i.e., 3.5 nm in diameter and 1.0 nm in height) giving rise to a structure sensitivity of the oxidation of carbon monoxide.

Concerning the nature of active sites, the above-described in-depth characterization showed EPR signals for F-centers in Au/ZrO_2-F and Au/TiO_2-SG together with CESR signals of small gold particles in the former, whereas in the latter, dipolar interaction of the Au particles with the F-centers of the support gave rise to a line broadening that probably prevented CESR signal detection. Paramagnetic F-centers, i.e., electrons trapped in oxygen vacancies, have strong one-electron donating character.[46] Obviously, by reduction of the catalysts in hydrogen, electron transfer takes place from the reduced support to gold particles and should, in principle, also be possible from this support to the organic reactant during reaction. Note, that $Au^{\delta-}$ sites exposed at the surface of small negatively charged gold clusters were found in Au/TiO_2 beside Au^0 sites exposed at the

(42) (a) Che, M.; Bennett, C. O. *Adv. Catal.* **1989**, *36*, 55−172. (b) Bond, G. *Chem. Soc. Rev.* **1991**, *20*, 441−475. (c) Bond, G. *Acc. Chem. Res.* **1993**, *26*, 490−495.

(43) Claus, P.; Hofmeister, H. *J. Phys. Chem. B* **1999**, *103*, 2766−2775.

(44) Englisch, M.; Jentys, A.; Lercher, J. A. *J. Catal.* **1997**, *166*, 25−35.

(45) (a) Delbecq, F.; Sautet, P. *J. Catal.* **1995**, *152*, 217−236. (b) Delbecq, F.; Sautet, P. *J. Catal.* **1996**, *164*, 152−165.

(46) Winiarek, P.; Kijenski, J. *J. Chem. Soc., Faraday Trans.* **1998**, *94*, 167−172.

Table 3. Catalytic Results[a]

catalyst	$\bar{d}_{Au}$ (nm)	activity (mmol g_{Au}^{-1} s^{-1})	E'_A[c] (kJ mol^{-1})	selectivity[b] (%) AyOH	PA	PrOH	HC	OP	ref
Au/TiO_2-DP	5.3	513	58	23	58	5	5	9	*d*
Au/TiO_2-I	2.0	400	60	26	47	11	10	6	*d*
Au/TiO_2-SG	1.1	2	34	19	79	2			*d*
Au/ZrO_2-F	1.4	41	17	19	78		3		*d*
Au/ZrO_2-DP	3.8[e]	54	29	43	56		1		39

[a] Overall activity at $T = 513$ K, $p_{total} = 2$ MPa, H_2/acrolein = 20, and $W/F^o_{Ac} = 15.3$ g h mol^{-1}. [b] Selectivity to AyOH (allyl alcohol), PA (propanal), PrOH (1-propanol), HC (hydrocarbons: ethane, ethylene, propane, propene), and OP (other products: acrylic acid, formyldihydropyran). [c] Apparent activation energy. [d] This work. [e] Bimodal particle size distribution (2.1 *and* 7.4 nm)[39].

surface of small three-dimensional particles.[47] By an electron transfer due to the interaction of nanosized gold particles and F-centers, gold is expected to become enriched in valence electron density, thereby altering the interaction of the active sites with the functional group and facilitating a partial transfer of electron density to the π^* orbital of the unsaturated bond. A similar situation is encountered, e.g., for the adsorption of the olefinic double bond of ethene on electron-rich silver.[48] For the hydrogenation of α,β-unsaturated aldehydes, an increase of the specific reaction rate of the C=C bond with increasing occupation of the d-orbitals of the metal and, hence, with increasing polarity of the metal−hydrogen was observed so that the reaction of atomically chemisorbed hydrogen with the olefinic group was claimed to proceed as nucleophilic ligand addition.[49] On the other hand, theoretical calculations in line with many experimental results indicated that a higher charge density on metal surface atoms decreases the binding energy of the olefinic double bond via an increase of the repulsive four-electron interaction and favors the back-bonding interaction with the π^*_{CO} orbital to a larger extent than with π^*_{CC} orbital, so that the hydrogenation of the C=O group should be favored over that of the C=C group.[2,45] In terms of the frontier orbital (HOMO−LUMO) model, the Fermi energy is increased by such an electron transfer. However, if quantum size effects occur, a decreasing density of occupied states within the HOMO (in terms of the band model: narrowing of the valence band, d band) induces a decreasing repulsion because of lowering the probability of interaction between orbitals ψ of the surface and the discrete adsorbed molecules[50] according to

$$E_{repulsion} \approx \sum_{i,j}^{occ} |\langle \Psi_i^{metal} | \Psi_j^{ads} \rangle|^2 \qquad (4)$$

This should lead to an overall decrease of repulsion[50] enabling preferred hydrogenation of the C=C group on quantum-sized systems (Au/ZrO_2-F, Au/TiO_2-SG). Furthermore, a lower density of states in the HOMO should induce a lower probability of back-donation, resulting in a decrease of C=O adsorption and, thus, in a lower selectivity to the unsaturated alcohol. On the other hand, for larger gold particles (Au/TiO_2-DP, Au/TiO_2-I), the C=O hydrogenation is markedly enhanced, as described in detail above.

Note, that besides the η^2-(C,C) and η^2-(C,O) adsorption geometries according to the classical Horiuti−Polanyi mechanism, acrolein could also be activated through a competing η^4-(C,C,C,O) mode which gave π-allylic and oxo-π-allylic intermediates as half-hydrogenated surface species determining the formation of the unsaturated alcohol and the saturated aldehyde, respectively.[1] The η^4-(C,C,C,O) adsorption mode may be advantageous on electron-rich metal in terms of the delocalization of electrons[51] and involves the carbonyl oxygen atom interacting with support cations at the interface between gold nanoparticles and TiO_2 or ZrO_2. In this case, allyl alcohol formation is favored through the cooperative effect of special active sites comprising Ti^{4+} or Zr^{4+} ions or defect sites as Ti^{3+} or Zr^{3+}, as evidenced in this study and negatively charged gold nanoparticles anchored on closely neighboring F-centers.

In the case of TiO_2- and ZrO_2-supported Pt catalysts, the electronic metal−support interaction and the microscopic nature of the active sites were investigated by Yoshitake and Iwasawa[52] by X-ray absorption near-edge spectroscopy (XANES) where a decrease of the unoccupied d density of Pt, to a degree dependent on the type of the support, was observed after high-temperature reduction (at 773 K) of the catalysts. ZrO_2 donates electrons to Pt without migration of support oxide. Furthermore, under the conditions of ethene hydrogenation, the electrons, transferred from ZrO_2 to Pt, were extracted by di-σ-adsorbed ethylene, being negatively charged,[52] and thus, ethylene is electron accepting on Pt/ZrO_2. This electron acceptor effect of the C=C bonding could also be involved in the adsorption and hydrogenation of acrolein on the smallest, 1.4 and 1.1 nm, gold nanoparticles supported on ZrO_2 and TiO_2.

Regarding the role of hydrogen, it is noteworthy that in the case of Au/TiO_2 evidence by FTIR were reported[47] that H_2 dissociates on nanosized gold, producing atomic hydrogen that may react with adsorbed acrolein or reduce support surface sites upon spillover. The reduction of the catalyst support, at a far lower temperature (573 K) than normally required for the occurrence of (strong) metal−support effects (>700 K), was clearly evidenced by EPR in this study (see section on Quantum Size Effects). There is evidence that surface mononuclear organometallic complexes are also capable of activating and reacting with molecular hydrogen from the gas phase: For example, gold hydrogenates a strongly complexing strained alkene such as norbornene which may indicate that it is the π-complex activating the hydrogen.[53]

Finally, comparative electron microscopy and DRIFTS studies of Au/ZrO_2 and Au/TiO_2 by Baiker et al.[54] recently showed that, despite similar gold particle sizes, the catalytic properties in the CO oxidation are quite different. That means that apart from the gold particle size other factors seems to be crucial for

(47) Boccuzzi, F.; Chiorino, A.; Manzoli, M.; Andreeva, D.; Tabakova, T. *J. Catal.* **1999**, *188*, 176−185.
(48) Wang, P.-K.; Ellis, P. D. *J. Am. Chem. Soc.* **1991**, *113*, 9675−9676.
(49) Dinse, M.; Kripylo, P. *Chem. Tech.* **1992**, *44*, 249−252.
(50) van Santen, R. A.; M. Neurock, M. *Catal. Rev.-Sci. Eng.* **1995**, *37*, 557−698.
(51) (a) Yoshitake, H.; Iwasawa, Y. *J. Catal.* **1990**, *125*, 227−242. (b) Yoshitake, H.; Asakura, K.; Iwasawa, Y. *J. Chem. Soc., Faraday Trans. 1* **1989**, *85*, 2021−2034.
(52) Yoshitake, H.; Iwasawa, Y. *J. Phys. Chem.* **1992**, *96*, 1329−1334.
(53) (a) Amir-Ebrahimi, V.; Rooney, J. J. *J. Mol. Catal.* **1991**, *67*, 339. (b) Patterson, W. R.; Rooney, J. J. *Catal. Today* **1992**, *12*, 113−129.
(54) Grunwaldt, J.-D.; Maciejewski, M.; Becker, O. S.; Fabrizioli, P.; Baiker, A. *J. Catal.* **1999**, *186*, 458−469.

catalytic activity of supported gold catalysts. The better activity of Au/TiO_2 in this oxidation reaction was explained by the number of low-coordinated gold sites being higher on TiO_2 than on ZrO_2 due to different support interactions causing different particle shapes. However, similar changes of the shape of gold particles could not be detected with TEM/HREM in the samples of the present study.

Conclusions

Nanostructural and catalytic properties in partial hydrogenation of acrolein have been studied for gold particles in the diameter range of 1−5 nm deposited on titania and zirconia. Catalyst activity and selectivity to the desired allyl alcohol are increased with increasing gold particle size. We conclude that adsorption of the C═O group of the α,β-unsaturated aldehyde is favored by face atoms, so that most likely the increased fraction of dense (111) planes of the larger gold particles will give higher formation rates of allyl alcohol than low-coordinated atoms of smaller sized gold particles. However, from structural analysis by TEM/HREM and in-depth characterization with EPR, we conclude that the influence of small gold particles on the intramolecular selectivity of the hydrogenation of conjugated functional groups originates from active sites comprising paramagnetic F-centers of strong one-electron donating character and electron-rich gold particles. The origin of the antiphatetic structure sensitivity of the hydrogenation of the C═O vs C═C group may be attributed to quantum size effects which alter the electronic properties of sufficiently small gold particles. Thus, nanosized gold particles on oxide support prepared by appropriate methods open new prospects to adjust within wide limits material properties for the design of heterogeneous catalysts.

Acknowledgment. This work has been supported by the Federal Ministry for Science and Education under Grant 03D0028A0. P.C. thanks the Fonds der Chemischen Industrie for financial support. P.C. and C.M. are grateful to M. Lucas (Berlin) for performing the catalytic measurements.

JA0012974